Multi-Dimensional Computer Simulation of MHD Combustor Hydrodynamics

ANL/CP--72897

DE91 011851

G. F. Berry, S.L. Chang, S.A. Lottes, and W. A. Rimkus

ARGONNE NATIONAL LABORATORY
Energy Systems Division
9700 South Cass Avenue
Argonne, Illinois 60439

Manuscript submitted to
American Institute of Aeronautics and Astronautics
June 24-26, 1991
Honolulu, Hawaii

April 4, 1991

MULTI-DIMENSIONAL COMPUTER SIMULATION OF MHD COMBUSTOR HYDRODYNAMICS

G. F. Berry, S.L. Chang, S.A. Lottes, and W. A. Rimkus
Argonne National Laboratory
9700 South Cass Avenue
Argonne, Illinois 60439

ABSTRACT

Argonne National Laboratory is investigating the non-reacting jet-gas mixing patterns in an MHD second stage combustor by using a two-dimensional multi-phase hydrodynamics computer program and a three-dimensional single-phase hydrodynamics computer program. The computer simulations are intended to enhance the understanding of flow and mixing patterns in the combustor, which in turn may lead to improvement of the downstream MHD channel performance.

A two-dimensional steady state computer model, based on mass and momentum conservation laws for multiple gas species, is used to simulate the hydrodynamics of the combustor in which a jet of oxidizer is injected into an unconfined cross-stream gas flow. The model predicts jet-gas mixing patterns by computing the velocity and species concentration distributions in the combustor. In this paper the effects of parametric variation of jet angle and flow asymmetry on the mixing patterns are summarized. The modeling is intended to determine better mixing patterns for the combustor design because improved mixing can increase combustion efficiency and enhance MHD generator performance. A parametric study reveals that (1) non-reacting jet-gas mixing strongly depends on jet angle for coflow injection (jet angle < 90 degrees), (2) counterflow jets have better mixing than coflow jets, and (3) asymmetry of the inlet gas flow affects the mixing pattern, but only has a minor effect on the mixedness at the chamber exit.

A three-dimensional code is used to examine the effects of the side walls and the distributed jet flows on the non-reacting jet-gas mixing patterns. The code solves the conservation equations of mass, momentum, and energy, and a transport equation of a turbulence parameter and allows permeable surfaces to be specified for any computational cell.

The computer code treats the two different fluids in the combustor by assigning two different temperatures for each flow and using local temperature to represent the mixture ratio. To allow jet penetration in a cross-stream direction, a jet entry model was developed. The entry model uses a one-cell nonpermeable channel next to each jet port to allow the jets to be specified with a velocity, controlled by the surface permeability of the entry channel. In general, the jets penetrate deep into the main flow and a large interface area is rapidly formed between jets and main flow promoting a high rate of convective mixing. Once the jets are turned in the downstream direction, mixing slows down dramatically as the steep gradients between jet and gas streams decay. Further mixing occurs primarily in turbulent and diffusive transport processes as the flow moves downstream. These gradient driven processes may be helped or hindered by the pattern of secondary flows established in the cross-stream through jet interaction as a consequence of jet port arrangement. Those arrangements which lead to the establishment of secondary flows or vortices in the cross-plane that sweep through the chamber corners appear to have the highest combined rates of thermal and momentum mixing.

NOMENCLATURE

A	Cross-sectional area in Y-Z plane (m^2)
C	Mass ratio of local jet to total mixture
D	Combustor 2d-width or 3d-hydraulic diameter(m)
F	Local jet concentration (or flux)
H	Combustor height (m)
k	Turbulent kinetic energy (J/kg)
L	Combustor length (m)
L_j	Jet port location in X-coordinate (m)
S	Source terms in conservation equations
T	Temperature (K)
u	Velocity (m/s)
U_0	Inlet velocity (m/s)
U	Velocity in X-direction (m/s)
V	Velocity in Y-direction (m/s)
W	Velocity in Z-direction (m/s)
X	Axial displacement coordinate (m)
Y	Vertical displacement coordinate (m)
Z	Horizontal displacement coordinate (m)

Greek Letters

β	Normalized temperature difference
ε	Turbulence dissipation (J/kg-s)
ϕ	General dependent variable
Γ	Diffusion coefficient (turbulent and laminar)
ρ	Density (kg/m^3)
σ	Normalized cross-sectional deviation
τ	Average cross-sectional value

Subscripts

i,j	Summation index from 1 to 3

INTRODUCTION

A magnetohydrodynamic (MHD) power plant depends upon the interaction between magnetic fields and an electrically conducting fluid flow to generate electrical power, a process which can attain higher overall efficiency and produce less pollutants compared to a conventional coal-fired power plant [1-2]. Under the sponsorship of the U.S. Department of Energy, TRW is developing a 50 MWt MHD combustor [3]. The combustor is essentially a two-stage gasification device upstream of the MHD generator. The first stage consists of a swirling pulverized coal gasification section followed by a deswirl section where ionizing seed is injected into the gas stream. The gasification section removes most of the slag and the deswirl section provides an outflow with minimal velocity profile distortion. Heat loss and NOx formation are minimized in the first stage by operating at a low equivalence ratio. The second stage combustor following the first stage deswirl section includes oxidizer injectors and a combustion chamber. Oxidizer is added in the second stage to obtain the desired plasma stoichiometry and temperature.

Among several important issues regarding the performance of the the second stage combustor, the penetration and mixing characteristics of oxidizer jets injected into a crossflow are considered paramount. The jet-flow mixing in the second stage combustor has a large effect on the downstream generator performance. One of the major concerns is the distortion of the gas temperature profiles caused by poor mixing which may significantly lower the effective electric conductivity of the gas.

Tests have been performed to evaluate the effects of the non-uniformity of mixture temperature and velocity in the second stage combustor on the MHD channel performance. Poor jet penetration and jet-gas mixing are believed to be mainly responsible for the non-uniformity. Good mixing between the first stage sub-stoichiometric combustion products (or gas flow) and the oxidizer jets (or jet flow) would promote more uniform and complete combustion in the second stage of the MHD combustor [4,5].

Holdeman and Walker [6] and Rudinger [7] developed empirical models to predict penetration and mixing characteristics of jets in a confined crossflow based on experimental data and a self-similar flow principle. Scaling parameters like momentum flux ratio, mass ratio, and density were used to correlate the penetration and mixing parameters. In recent years, some numerical solutions of the deflected-jet situations have been reported. Patankar, Basu, and Alpay [8] used a comprehensive three-dimensional turbulent flow computer model and predicted the velocity field generated by a round jet deflected by a main stream normal to the jet axis with some success.

Experimental cold flow studies of the flow and mixing patterns in the second stage of a MHD coal-fired combustor have been conducted by TRW [9-11]. A one-third scale transparent model of the 50 MWt combustor was used. To determine the degree to which the secondary oxidizer mixes with the combustion products from the first stage, injector concentration measurements were taken throughout the flow cross-section at several axial stations downstream of the injector frame. To compare with the experimental measurements and enhance the understanding of combustor performance, Argonne National Laboratory (ANL) used a two-dimensional combustion computer code and a three-dimensional hydrodynamics computer code to investigate the flow mixing processes in the MHD second stage combustor. The two-dimensional combustion code was used to simulate the two-fluid mixing processes where the jet angle was the primary variable with the combustion process to be studied in the next portion of this ongoing investigation, while the three-dimensional code was used to study non-reacting jet penetration and jet-gas mixing patterns where the jet arrangement was the primary variable. This paper presents two- and three-dimensional hydrodynamic results and discusses the significance and relationship between these two complementary studies.

COMPUTER SIMULATION

Over the past decade, the research team of Argonne National Laboratory and University of Illinois at Chicago has developed models and associated computer codes for predicting mixing and combustion processes in air-breathing and liquid-rocket engines [12-14]. The computer code used for the two-dimensional computation in this paper is a general multi-phase, multi-species, turbulent combustion code. General conservation laws, expressed by elliptic-type partial differential equations, are used in conjunction with rate equations governing the mass, momentum, species, turbulent kinetic energy, and turbulent dissipation for the isothermal nonreacting flow case under investigation.

For convenience in numerical solution the conservation equations can be put in the form:

$$\nabla \bullet (\rho U \phi - \Gamma_\phi \nabla \phi) = S_\phi$$

The general flow variable, ϕ, is a member of the set $\{1, U, V, C, k, \varepsilon\}$. A k-$\epsilon$ turbulence model [15] is used to model the effects of the turbulence in the flow field. A detailed description of the computer code is given in reference 13.

Flow variables are assigned values at the inlet plane and jet openings in the side walls. A reference pressure is assigned

at the midpoint of the inlet plane. Patankar's [16] locally one way flow assumption is applied to the outflow boundary, eliminating the need to specify the values of flow variables at the outflow boundary. In this formulation, the streamwise diffusion coefficients are taken to be zero at the outflow boundary. The side walls are impermeable. A momentum wall function [15] is used to bridge the near wall boundary layer.

To compare different test cases with the same jet mass flow rate, the mass flow rate of the jets as well as velocity is specified from the input conditions. The jet mass flow rate is determined from the reference pressure, the specified velocity, and initial area of the jet inlet. This initial jet mass flow rate is retained in the solution by adjusting the width of the jet opening during the solution procedure to account for the difference between the reference pressure and the solved for pressure at the jet opening. The difference can be up to a few percent in the cases included in this study.

The mean and standard deviation of jet concentration or jet flux, used for describing the mixing development in the primary flow direction (or X-direction), are defined as follows:

Cross-Sectional Mean

$$\tau(X) = \iint F \, dA / A$$

Normalized Cross-Sectional Standard Deviation

$$\sigma(X) = [\iint (F - \tau)^2 \, dA / A]^{1/2} / \tau$$

where F can be either jet concentration or jet flux.

The standard deviation of jet concentration or flux is used as an indicator of jet-main flow mixing because it is maximal where the jet and main flows are completely separated and is zero where they are homogeneously mixed. In general, the normalized standard deviation monotonically decreases as the mixing process proceeds along the main flow direction.

Figure 1 shows the combustor under investigation, an idealized rectangular box consisting of four solid side walls (front, back, top and bottom), a main gas inlet (left), twelve jet injection holes on both top and bottom walls, and the mixture exit (right). The two-dimensional computational domain is defined in a cross-sectional area (dotted line area in Figure 1) in the middle of the combustor away from the viscous effects near the front and back walls. Two narrow openings on top and bottom walls, representing distributed injection holes, are adjustable during computation so that both the total jet mass flow rate and jet velocity can be defined by input values. When the jet velocity is specified at the jet inlet, the compressibility of jet inlet conditions affects the mass conservation of jet flow because pressure is no longer a free boundary condition, but rather needs to be determined from the flow solution in the interior. A procedure added to the computer code dynamically alters the computational grid to adjust the area of the jet during iteration toward the solution in such a way that the jet mass flow rate computed matches the input value. Figure 2 shows a two-dimensional grid point system having 46 by 21 interior nodes, for which a coordinate system with an origin at the lower left corner, a horizontal X-axis, and a vertical Y-axis is defined. The evenly spaced grid points are used for the Y-axis and variably spaced grid points are defined for the X-axis depending on the jet location. Dense grid points are selected near the jet opening where large flow property gradients are expected.

In a typical computation, the mass residual of each cell in the computational domain is checked after each iteration of solving mass, momentum and energy equations. The mass residual is required to be smaller than a preset convergence criterion before stopping the iteration. If the process converges, mass residual becomes smaller as the iteration goes on. Each iteration takes approximately 0.25 second of computing time and a typical convergent case needs about 200 seconds of supercomputing time to reduce the maximum normalized mass residual to less than 10^{-9}.

The COMMIX code developed at ANL [17] solves the conservation equations of mass, momentum, and energy, and a transport equation of a turbulence parameter. The conservation equations possess a common form. If one denotes the general dependent variable, ϕ, to represent a scalar 1 in the continuity equation, three velocity components, u_i, i=1, 2, and 3, in momentum equations, enthalpy, h, in energy equation, and turbulent kinetic energy, k, in a one-parameter turbulence model, the conservation equations have the following form in a Cartesian coordinate system.

$$\partial(\rho u_j \phi)/\partial X_j = \partial(\Gamma_\phi \, \partial\phi/\partial X_i)/\partial X_i + S_\phi$$

The equations are solved by using a fully implicit algorithm in a staggered grid system. The details of the COMMIX code are described in reference 17.

Two different fluids (gas and jet) are mixed in the combustor. The COMMIX code can treat only one fluid in its solution procedure. Two different temperatures are chosen to distinguish the main flow from the jet flow. The COMMIX code computes enthalpy (or temperature) of a computational cell by averaging the enthalpies of both jet and main flows in the cell on a mass basis. If the jet temperature is higher than the main gas temperature, the mass fraction of the jet flow in a cell is primarily proportional to the temperature rise.

An important feature of the COMMIX code is that it allows the users to specify permeable surfaces for a

computational cell. To allow jet penetration in a cross-stream direction in a computer simulation, a jet entry model was developed. The jet entry model uses a one-cell non-permeable channel next to the injection port for each jet entry. The entry channel consists of four one-cell nonpermeable surfaces perpendicular to the jet flow direction and a partially permeable surface on the end of the channel. The jet entry model allows the jet to be injected into the cross-stream flow with a specified velocity, controlled by the surface permeability of the entry channel. The COMMIX code with this jet entry model was tested by comparing with the two-dimensional combustion computer code. The results showed good agreement.

The general variable F (for the three-dimensional treatment) can be either temperature or axial velocity. The lower the temperature or velocity deviation, the better is the thermal or axial momentum mixing. As the flows become perfectly mixed, the average temperature approaches the bulk temperature, the temperature deviation becomes zero, and the velocity deviation drops to that of a fully developed turbulent channel flow.

Figure 3 shows the idealized MHD second stage combustor under investigation. There are opposing jet ports on top, bottom, front, and rear walls. Jets on the top and bottom walls are referred to as vertical jets, while jets on the front and rear walls are referred to as horizontal jets. Four different 12-jet arrangements were investigated. One arrangement places 6 jets, evenly spaced, on each of the top and bottom walls (V1 to V6 of Figure 4). The other three arrangements have two jets on each of the front and rear walls at Y/D = 0.45 and 0.55 (H1 and H2 of Figure 4) and four jets on each of the top and bottom walls. The three arrangements with front and rear wall jet ports are called center, side, and mixed arrangements according to the position of jets on the top and bottom walls. These positions are derived by deleting pairs of opposing jets in the top and bottom walls (Figure 4). The center-jet arrangement deletes two pairs of jet ports V1 and V6, the side-jet arrangement deletes V3 and V4, and the stagger-jet arrangement deletes V2 and V5. Combustor geometry and simulation flow conditions are summarized in Table I.

Table I Combustor Geometry and Flow Conditions

Combustor Dimension (L:D:H) =	3.8:1:1
Jet Port Location (L_j/D) =	0.66
Pressure =	1 atm
Bulk Jet Concentration =	6.4 %
Jet Angle =	90 deg.
Jet Velocity =	614 m/s

The coordinate origin is set at the lower left corner of the inlet plane with X-, Y- and Z-axes in main flow (or axial), height (or vertical), and width (or horizontal) directions, as shown in Figure 3. A 41 by 21 by 13 grid system is defined for the computational domain of this geometry. For a symmetrical arrangement, only 41 by 11 by 7 nodes are used in the computation. Computation of a symmetrical case with good numerical convergence generally requires about 1600 seconds of CPU time on a CRAY/XMP supercomputer.

RESULTS AND DISCUSSION

A parametric study was conducted to investigate the effects of jet angle and inlet gas flow symmetry on the mixing pattern of the jet and the inlet gas flows. Results of the computer study indicate (1) jet-gas mixing strongly depends on jet angle in the jet angle range of 40-90 degrees, (2) counterflow jets have better jet-gas mixing and mixing is relatively insensitive to jet angle (angle > 90 degrees), and (3) asymmetry of the inlet gas flow affects the mixing pattern but has only a small effect on the extent of jet-gas mixing over the chamber length.

Effect of Jet Angle on Flow and Mixing Patterns

The jet angle is defined as the angle between the jet velocity vector and the positive X-axis. Computations with jet angles ranging from 40 to 140 degrees were performed to simulate the mixing pattern; conditions for these runs are summarized in Table II.

Table II Simulation Conditions

Inlet Reynolds Number =	1.1×10^5
Jet Velocity =	$13.7\ U_0$
Pressure =	1 atm
Temperature =	20 C

The computed flow and mixing patterns for the two cases of 50 and 130 degree jet angle are shown in Figures 5 and 6, respectively. For each case, part "a" of the figure shows velocity vectors and part "b" shows contours of jet concentration.

For a 50 degree jet angle case, jet penetration is shallow, and consequently a region of strong convective mixing exists around the jet opening but the jet-gas mixing over the chamber width is poor. In a region from the jet opening to the exit, the jet flows are pushed toward the walls by the main gas flow. In this region, flow velocity is higher in the outer regions and lower in the central region, and the jets are confined in a thick layer near the walls, as shown in Figures 5a and 5b. The shear layer between the high speed jet flow and the low speed gas flow is responsible for the further mixing of the two flows by turbulent and viscous momentum transport. The shear layer is not fully developed in the combustor, evidenced by the low exit velocity in the middle as shown in Figure 5a. The 5% jet

concentration contour reaches the center line of the combustor at about X/D = 3.1 as shown in Figure 5b.

For a 130 degree jet angle case, the jet penetration is deeper and mixing is better compared with the 50 degree jet angle case. Convective jet penetration is the dominant process responsible for jet-gas mixing. Vortices are found right after the jet opening as shown in Figure 6a. The 5% jet concentration contour reaches the center line of the combustor at about X/D = 1.9 as shown in Figure 6b. In Figure 6a, the exit velocity profile is highest in the middle.

Figure 7 shows the axial development of the jet-gas mixing for three cases, 50, 100, and 130 degree jet angle. Figure 7a plots the mean jet mass concentration versus the axial (or X-axis) displacement and Figure 7b plots the normalized jet concentration standard deviation versus the axial displacement. A reference jet concentration is defined as the jet concentration of a uniform mixture of jet and gas.

For the 50 degree jet angle case, mean jet concentration increases along the X-axis and reaches about 0.14 at the exit as shown in Figure 7a. The exit mean jet concentration is lower than the reference jet concentration because the high jet concentration zones match the high velocity zones as shown in Figure 5. In Figure 7b, the normalized jet concentration standard deviation for 50 degree injection decreases from about 2.6 near the injection location to about 0.6 at the exit. The standard deviation indicates the location of a rapid convective mixing zone followed by a much slower diffusive mixing zone. The convective mixing zone is near the jet opening and mixing is primarily due to jet penetration.

For the 100 degree jet angle case, the mean jet concentration has a maximum value near X/D = 1 as shown in Figure 7a. The exit mean jet concentration is higher than the reference amount, indicating lower jet concentration in higher velocity zones. The normalized jet concentration standard deviation at the exit plane is about 0.2, much lower than that of the 50 degree case. With better jet penetration, the mixing is much more complete at the end of the convective mixing zone than in the 50 degree jet angle case.

For the 130 degree jet angle case, the curves of mean jet concentration and jet concentration standard deviation are similar to those of the 100 degree case. The mean is higher than those of the 50 degree and the 100 degree cases. The deviation is much lower than that of the 50 degree case and is close to that of the 100 degree case. The jet has a large velocity component counter to the main flow direction at the injector location. The injected jet mass penetrates the upstream flow, is turned, and is brought back downstream by interaction with the main flow. This flow configuration produces the sharp peak in mean jet concentration just upstream of the injector location shown in Figure 7a. Much of the mixing in this case occurs upstream of the injector plane. Figure 7b shows that the normalized standard deviation of jet mass concentration is about 0.7 at the injection plane for 130 degree injection, while the value for 100 degree injection is about 1.3.

For comparison, the exit velocity and jet concentration of these three cases are plotted in Figure 8. The exit velocity of the 50 degree case has double humps near the walls and the exit velocities of the other two cases maximize at the center as shown in Figure 8a. The exit jet concentrations of the 100 and 130 degree cases seem more uniform than that of the 50 degree case as shown in Figure 8b. Because of different exit velocity profiles, the exit mean jet concentrations differs for various jet angles. The exit mean jet concentration for various jet angles are compared in Figure 9a. The exit mean jet concentration for jet angles smaller than 60 degrees is less than the reference jet concentration and for jet angles larger than 80 degrees it is greater than the reference jet concentration. In Figure 9b, the normalized standard deviation of jet flux at the exit for various jet angles is plotted. Jet-gas mixing is better for jet angles larger than 90 degrees. Jet-gas mixing depends strongly on jet injection angle for angles in the range 40 to 90 degrees, and the mixing rate increases with increasing injection angle. Above 90 degrees, the mixing rate is near optimum and only weakly dependent on injection angle.

Asymmetric Flow and Mixing Patterns

In general, the inlet gas flow velocity is asymmetric about the center line because of the non-ideal deswirl process before entering the second stage MHD combustor. Figure 10 shows the velocity vectors and jet concentration contour plots for a 130 degree case in which the inlet axial velocity changes linearly from 1.1 U_0 near Y/D = 0 to 0.9 U_0 near Y/D = 1 and other conditions remain the same as in Table II. Comparing Figures 10 and 6 reveals that for the asymmetric inlet flow case, (1) the vortex near the bottom wall, Y/D = 0, becomes larger, and (2) both maximal exit velocity and minimal exit jet concentration shift to the upper half of the chamber. In the entrance region from the inlet to approximately X/D = 1, the resultant momentum of both the inlet and the jet flows in the lower half of the chamber yields a higher pressure field compared to the upper half flows, because of the higher mass flow rate and velocity of the opposed flows. Thus, a field makes the main flow turn toward the upper half chamber after the larger vortex is formed in the lower half chamber and the velocity peak shifts to the upper half chamber.

The effect of this flow pattern on exit plane velocity and jet concentration profiles can be seen in Figure 11. For jet-gas mixing, the asymmetric case has a more uniform profile in the lower half chamber and a less uniform profile in the upper half chamber. These competing conditions yield an overall degree

of jet-gas mixing which is about the same in the symmetric and asymmetric cases. The standard deviation of jet mass concentration divided by the mean is about 0.178 for the asymmetric case versus 0.167 for the symmetric case. The exit velocity profiles in Figure 11 show the shift of the peak toward the upper half chamber for the asymmetric case. This shift yields higher velocity in the upper half chamber and lower velocity in the lower half chamber. A consequence of the velocity shift is that the standard deviation of jet mass flux, proportional to product of concentration and velocity, increases more than the standard deviation of jet mass concentration between the symmetric and asymmetric cases. The standard deviation of jet flux divided by the mean flux went from 0.211 to 0.264, an increase of 25 percent for the asymmetric case. If uniform jet flux is an important exit condition, then the degree of symmetry of the inlet gas flow becomes much more important than if only the extent of mixing of jet mass with gas is considered at the exit plane.

In analyzing the results of the three-dimensional computations, the effects of the jet port arrangement on two types of mixing, thermal mixing and momentum mixing, are considered. The development of mixing patterns is presented in Figures 12 through 23 in the form of contour plots of normalized temperature difference, contour plots of normalized X-direction (or axial) velocity, and plots of velocity vectors composed of the Y and Z components of velocity. The plots are shown at four X positions downstream of the jet injection position. Normalized temperature difference is defined as,

$$\beta = (T - T_{gas})/(T_{\tau} - T_{gas})$$

where T_{gas} is the inlet gas temperature and T_{τ} is the mean temperature. Normalized axial velocity is defined as,

$$U = u / u_{\tau}$$

in which u_{τ} is the average cross-sectional axial velocity (about 22 m/s).

The boundary conditions for all cases, inlet mass flow rates, velocities, temperatures, pressures, etc. are the same, except for the jet port arrangement on the walls at X/D = 0.66. Differences in the development of jet mixing in the downstream are therefore due to the variation of jet port arrangement.

The development of mixing for the case of 12 vertical jets is shown in Figures 12 to 14. The contours plotted in Figure 12 are for the normalized temperature difference, β. Contours of β = 1 represent the mean fluid temperature. The region of minimum value of β near the center of Figure 12a is the region the jets have not penetrated at X/D = 1.0. The impingement of jets in the center produces a set of sandwiched layers of hot and cold fluid in the downstream direction (Figures 12b and 12c). This layering provides a large interface area between hot and cold fluid, promoting thermal mixing. At downstream position X/D = 3.67, Figure 12d, the regions where layering occurs are fairly thoroughly mixed (fluid temperature is very near the mean).

Momentum mixing patterns for axial momentum in the case of 12 vertical jets can be seen in Figure 14. The jets, which are all located on the top and bottom walls in this case, constitute an obstacle to the main flow near the top and bottom walls at the injection position. The response of the main flow to these obstacles is in part to accelerate through the center of the channel as it interacts with the jets. This process creates a large region in the midrange of the Y-coordinate where the axial momentum is high and regions near the top and bottom walls where the axial momentum is low.

The velocity vectors for velocity components in the Y-Z plane, Figure 13a, show the even spacing of the opposed jets in the upstream. When the jets impinge, the relatively close, even spacing does not allow any significant degree of turning within the Y-Z plane, and therefore almost no secondary flow develops in the Y-Z plane as the main flow moves downstream (Figure 14c and 14d).

In the next three cases four of the vertical jets on the top and bottom walls are blocked, and the four horizontal jet positions on the front and rear walls (Figure 4) are opened. The impinging horizontal jets provide Z-momentum, which when interacting with the Y-momentum of the vertical jets may produce significant secondary flow patterns or vortices in the Y-Z plane as the flow develops downstream of the jets.

For the case with horizontal jets combined with centered vertical jets, thermal mixing proceeds rapidly in the region where the jets penetrate. The center and middle of the sides near the walls develop into a region with relatively well mixed warmer fluid, while the corners retain cooler fluid with steeper temperature gradients (Figure 15). Part of the reason for relatively poor mixing in the corners can be seen in the development of the secondary flow pattern in the Y-Z plane (Figure 16). With no jet momentum to sweep fluid out of the corners in the Y-Z plane, the secondary flow pattern develops with two vortices in each quadrant of the Y-Z plane, a very weak vortex near the corner and a relatively strong vortex between jet entry positions in the walls and the center of the chamber.

Both of the cases with horizontal jets combined with either staggered or side vertical jets exhibit the development of a secondary flow in the Y-Z plane with one vortex in each quadrant that sweeps fluid out of the corners into the chamber center region (Figures 19 and 22). This secondary flow process

appears to aid both the thermal and axial momentum mixing. Figures 18, 20, 21, and 23 show the development of the mixing patterns downstream of the jets. In these cases by the last frame shown, at X/D = 3.67, a large portion of the central part of the chamber extending nearly to the walls and into the corners appears to be fairly well mixed.

Figure 24 shows a comparison of the normalized temperature deviation over a Y-Z plane versus position along the chamber length. All cases show a rapid drop in the cross-sectional temperature deviation just downstream of the jet port position. This rapid mixing region extends only a short distance downstream where the jets are penetrating the main flow. Farther downstream, mixing proceeds primarily through the much slower gradient driven processes of turbulent or viscous diffusion, with some convective mixing still proceeding as a result of the development of secondary flows or vortices in the Y-Z plane. The three cases where jets were positioned near the corners all show a lower normalized temperature deviation over the exit plane than the case with centered jets.

Figure 25 shows the normalized velocity deviation over a Y-Z plane for the four jet arrangements. These results show that the axial velocity deviations for the arrangements which combine horizontal with vertical jets are all considerably lower than for the arrangement that uses only vertical jets. By the exit plane the purely vertical jet arrangement has an axial velocity deviation over the exit plane that is much higher than for the other arrangements.

While the measure of thermal mixing of the purely vertical jet arrangement is comparable to the arrangements of side and staggered vertical jets combined with centered horizontal jets, the measure of axial momentum unmixedness is much higher for the purely vertical jet arrangement.

The interaction between the uniformly spaced vertical jets is rather weak, compared with the interaction of the jet with the gas flow. This result confirms that the two-dimensional result yields reasonable results with respect to mixing, except for evaluation of cross-plane mixing which does not appear to be significantly affected by jet angle.

CONCLUSION

A computer simulation program using comprehensive physical models to investigate the penetration and mixing characteristics of oxidizer jets injected into a crossflow in an MHD second stage combustor has been developed on ANL's CRAY X-MP supercomputer. The model computes the velocity and species concentration distributions in the combustor and predicts non-reacting jet-gas mixing patterns. The modeling helps improve understanding of the mixing patterns for the combustor and allows identification of design parameters which can improve combustion efficiency and enhance MHD generator performance. A parametric study using the 2D computer code was conducted to evaluate the effects of jet angle and inlet gas flow asymmetry on the mixing pattern of the jet and the inlet gas flows. The 2D findings include (1) jet-gas mixing strongly depends on jet angle for coflow injection (jet angle < 90 degrees), (2) counterflow jets have better jet-gas mixing and mixing is relatively insensitive to jet angle (angle > 90 degrees), and (3) asymmetry of the inlet gas flow affects the mixing pattern but has only a small effect on the level of jet mass mixing over the chamber length.

A three-dimensional hydrodynamics computer code was used to investigate the flow mixing processes in an MHD second stage combustor. The flow and mixing patterns of four different jet port arrangements, including a 12 vertical jet arrangement and arrangements with 4 horizontal jets and either 8 centered vertical jets, 8 side vertical jets, or 8 staggered vertical jets, were computed and compared. Jet momentum is large enough so that the jets penetrate deeply into the main flow in all cases. The penetrating jets rapidly form a large interface area between jets and main flow promoting a high rate of mixing just downstream of the injectors. This initial high mixing rate may be viewed as convective mixing since it is driven primarily by expansion of the jets into the crossflow of the main stream. Once jet penetration has reached a maximum and the jets are turned into the downstream direction, mixing slows down dramatically as the steep gradients between jet and gas streams decay. Further mixing occurs primarily in turbulent and diffusive transport processes as the flow moves downstream. These gradient driven processes may be helped or hindered by the pattern of secondary flows established in the cross-stream through jet interaction as a consequence of jet port arrangement. Those arrangements which lead to the establishment of secondary flows or vortices in the Y-Z plane that sweep through the chamber corners appear to have the highest combined rates of thermal and momentum mixing.

ACKNOWLEDGEMENT

This work was supported by U.S. Department of Energy, Assistant Secretary for Fossil Energy, under Contract W-31-109-ENG-38. The authors thank Mr. Paul Lissak for his assistance in preparing the figures.

REFERENCES

[1] "Open-Cycle Magnetohydrodynamic Electric Power Generation, M. Petrick and B. Ya. Shumyatsky, eds., joint report of Argonne National Laboratory and U.S.S.R. Academy of Science (1978).

[2] Listvinsky, G., J. Alpay, L. Hil, K. King, D. Paul, D.

Vanevenhoven, K. Natesan and D.Y. Wang, "Development of a Prototypical MHD Coal Combustor," Proc. of 24th Intersociety Energy Conversion Engineering Conference, Washington, D.C., 2:965-970 (August 6-11, 1989).

[3] "Coal-Fired MHD Combustor Development Project: Phase IIIB", DOE Report DE87003845 (1987).

[4] McClaine, A., J. Pinsley, and B. Pote, "Experimental Investigation on the Effects of the TRW Two-Stage Coal Combustor on the Performance of the AVCO Mk VI MHD Generator," Proc. of 24th Intersociety Energy Conversion Engineering Conference, Washington, D.C., 2:971-977 (August 6-11, 1989).

[5] Burkhart, T., G. Funk, R. Glovan, A. Hart, A. Herbst, J. Joyce, Y.M. Lee, S. Lundberg, and I. Stepan, "Coal-Fired MHD Topping Cycle Hardware and Test Progress at the Component Development and Integration Facility," Proc. of 23rd Intersociety Energy Conversion Engineering Conference, Denver, CO, 4:445-453 (July 31-August 5, 1988).

[6] Holdeman, J.D., and R.E. Walker, "Mixing of a Row of Jets with a Confined Crossflow," AIAA Journal, Vol. 15, No. 2, pp. 243-249 (1977).

[7] Rudinger, G., "Experimental Investigation of Gas Injection through a Transverse Slot into a Subsonic Cross Flow," AIAA Journal Vol. 12, No. 4, pp. 566-568 (1973).

[8] Patankar, S.V., D.K. Basu, and S.A. Alpay, "Prediction of the Three-Dimensional Velocity Field of a Deflected Turbulent Jet," Tran. of ASME, pp. 758-762 (Dec. 1977).

[9] Grove, A., et. al., "Cold Flow Modeling Study of Coal-Fired MHD Combustor," 26th Symposium on Engineering Aspects of Magnetohydrodynamics, Nashville, AL (1988).

[10] Grove, A., "Cold Flow Mixing Study of 50 MWt MHD Coal-Fired Combustor Second Stage," 27th Symposium on Engineering Aspects of Magnetohydrodynamics, Reno, NV (1989).

[11] Grove, A., et. al., "Cold Flow Mixing Study of an MHD Combustor Model Using Laser Velocimeter and Concentration Measurements," 28th Symposium on Engineering Aspects of Magnetohydrodynamics, Chicago, IL (1990).

[12] Zhou, X.Q., and H.H. Chiu, "Spray Group Combustion Processes in Air Breathing Propulsion Combustors," Paper AIAA-83-1323, AIAA/SAE/ASME 19th Joint Propulsion Conference, Seattle, Washington (1983).

[13] Lottes, S.A., "Unsteady Group Combustion," Ph.D. Thesis, University of Illinois at Chicago, Chicago, Illinois (1989).

[14] Jiang, T.L., and H.H. Chiu, "Advanced Modeling of Spray Combustion Process in Air Breathing Propulsion Combustors," AIAA-87-0067, AIAA 25th Aerospace Science Meeting, Reno, Nevada (1987).

[15] Launder, B.E., and D.B. Spalding, "The Numerical Computation of Turbulent Flows," Computer Methods in Applied Mechanics and Engineering, Vol. 3, pp. 269-289 (1974).

[16] Patankar, S.V., "Numerical Heat Transfer and Fluid Flow," McGraw-Hill Book Company (1980).

[17] Domanus, H.M., R.C. Schmitt, W.T. Sha, and V.L. Shah, "COMMIX-1A: A Three-Dimensional Transient Single-Phase Computer Program for Thermal Hydraulic Analysis of Single and Multicomponents Systems," NUREG/CR-2896, ANL-82-25 (1983).

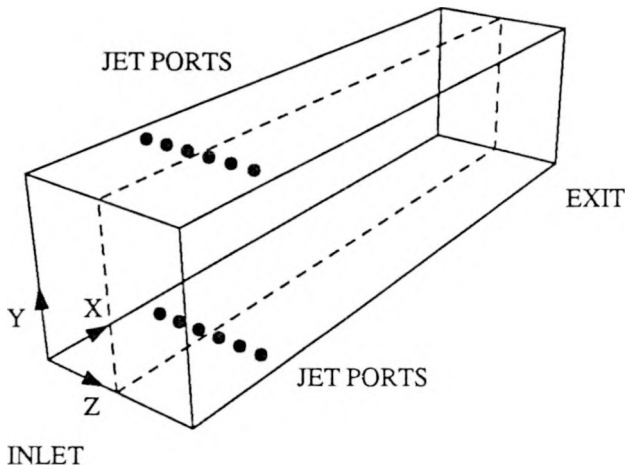

Figure 1 Idealized MHD combustor geometry, second stage, (12-jet)

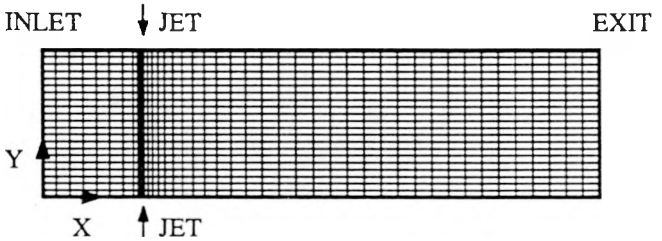

Figure 2 Two-dimensional grid system (46 by 21 nodes)

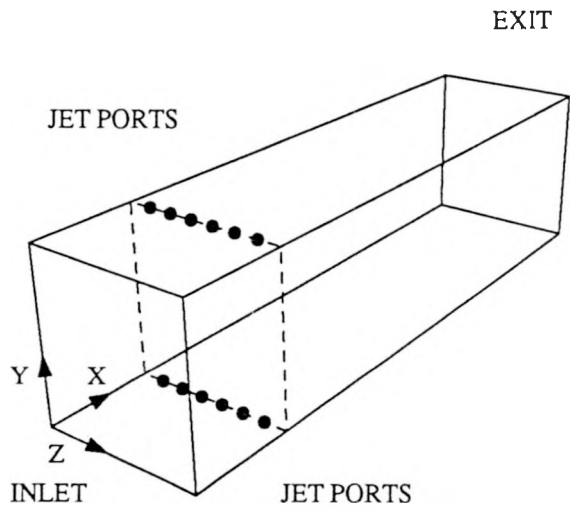

Figure 3 Idealized MHD combustor geometry, second stage, (12-jet)

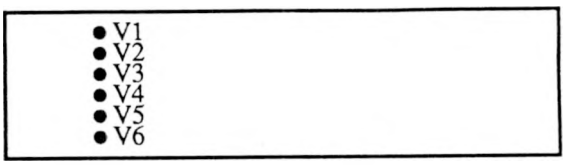

(a) Top wall

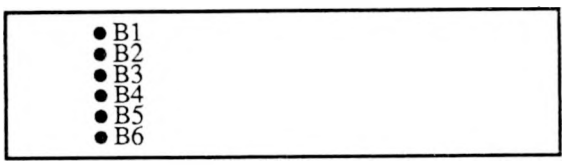

(b) Bottom wall

Figure 4 Jet port locations

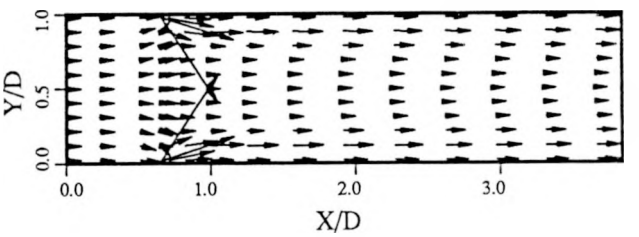

(a) Velocity vectors

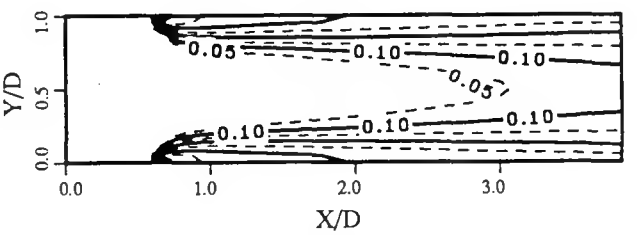

(b) Jet concentration contours

Figure 5 Flow and mixing patterns (50 Degree jet angle)

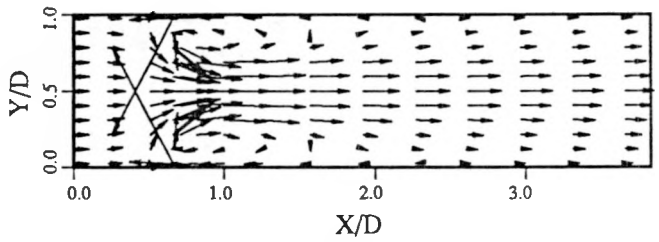

(a) Velocity vectors

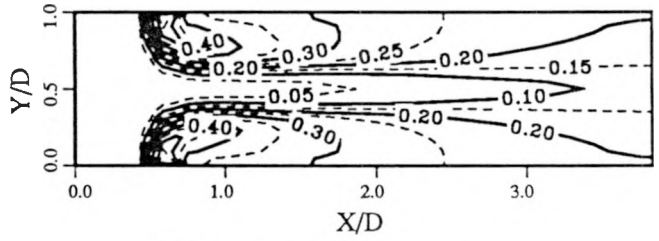

(b) Jet concentration contours

Figure 6 Flow and mixing patterns
(130 Degree jet angle)

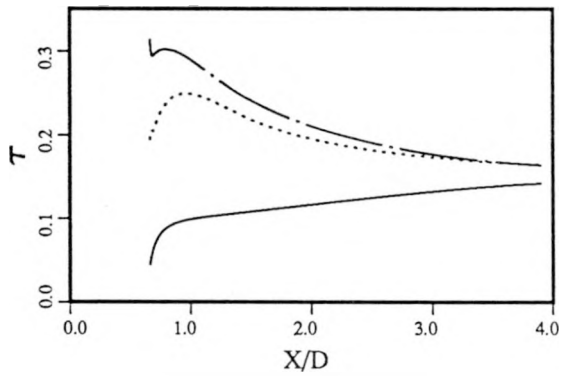

(a) Mean jet concentration

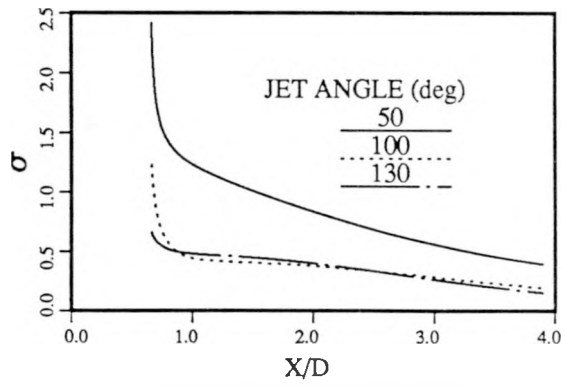

(b) Deviation of jet concentration

Figure 7 Axial development of symmetric jet-gas mixing for various jet angles

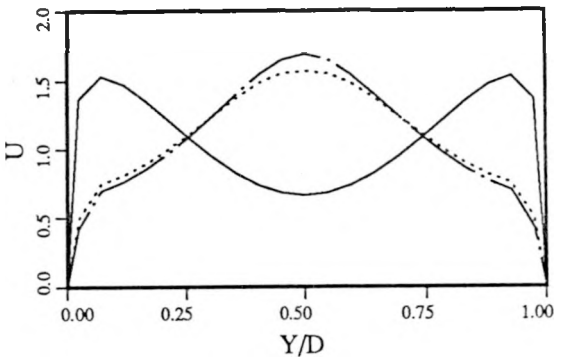

(a) Exit axial velocity

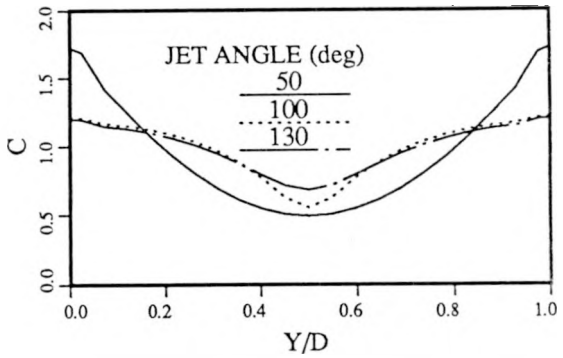

(b) Exit jet concentration

Figure 8 Normalized exit flow and mixing profiles for various jet angles

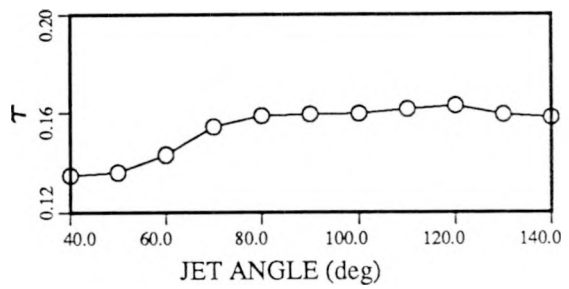

(a) Mean jet concentration

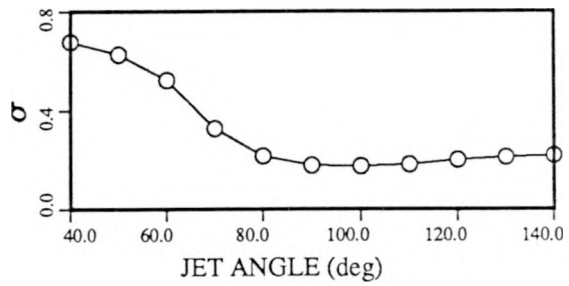

(b) Deviation of jet concentration

Figure 9 Effect of jet angle on jet-gas mixing at the exit

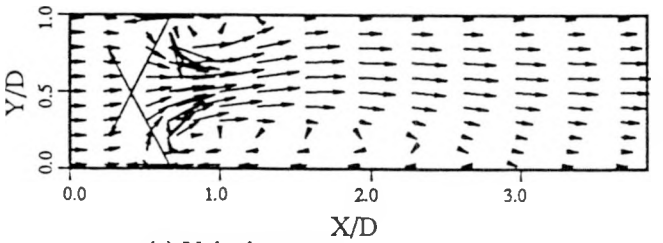

(a) Velocity vectors

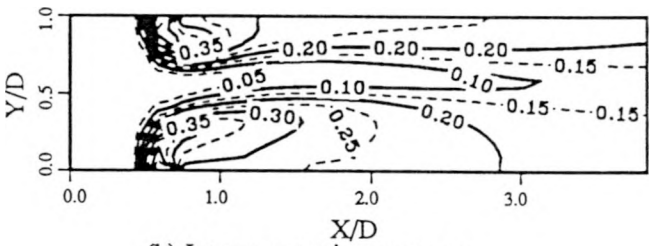

(b) Jet concentration contours

Figure 10 Asymmetric flow and mixing patterns

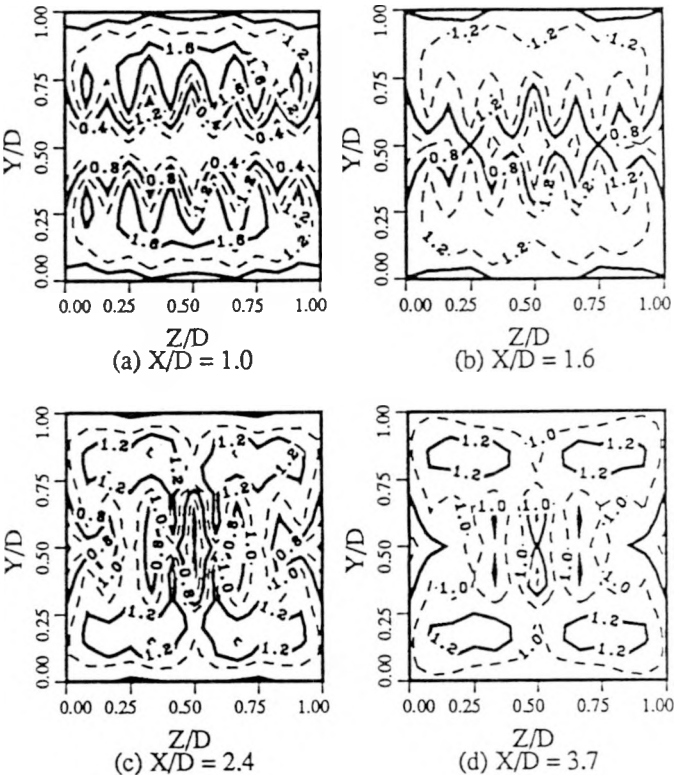

(a) X/D = 1.0 (b) X/D = 1.6

(c) X/D = 2.4 (d) X/D = 3.7

Figure 12 Development of thermal mixing
(β contours, 12-impinging-jet)

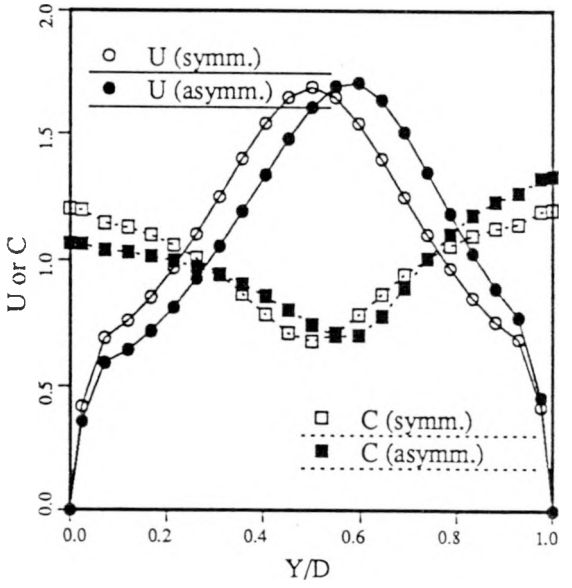

Figure 11 Exit flow and concentration profiles
for symmetric and asymmetric flows

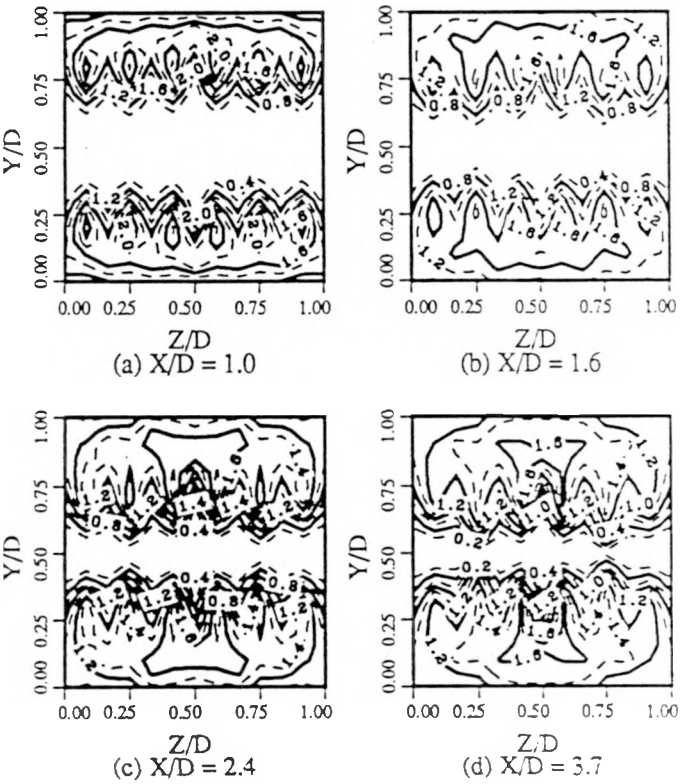

(a) X/D = 1.0 (b) X/D = 1.6

(c) X/D = 2.4 (d) X/D = 3.7

Figure 13 Development of thermal mixing
(β contours, 12-nonimpinging-jet)

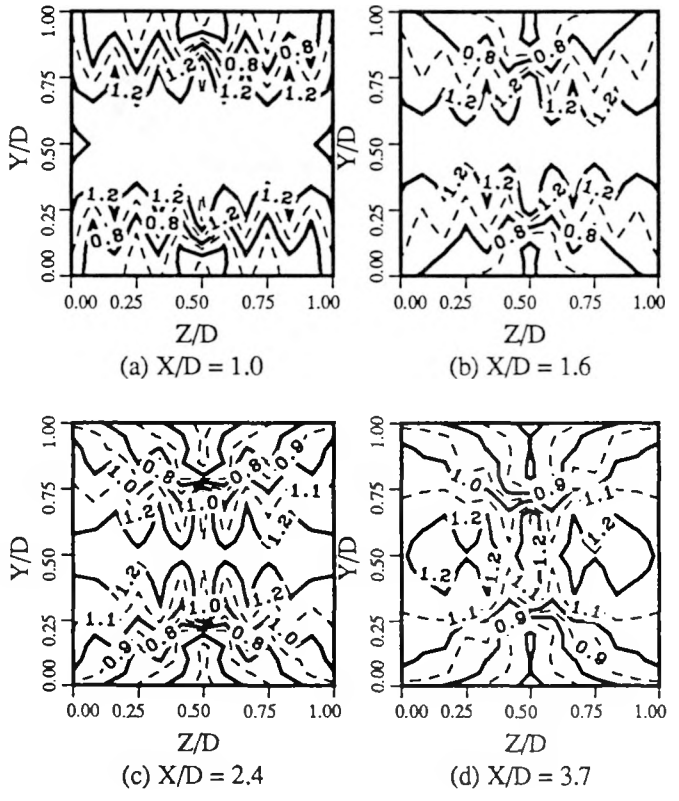

Figure 14 Development of momentum mixing
(U contours, 12-vertical-jet)

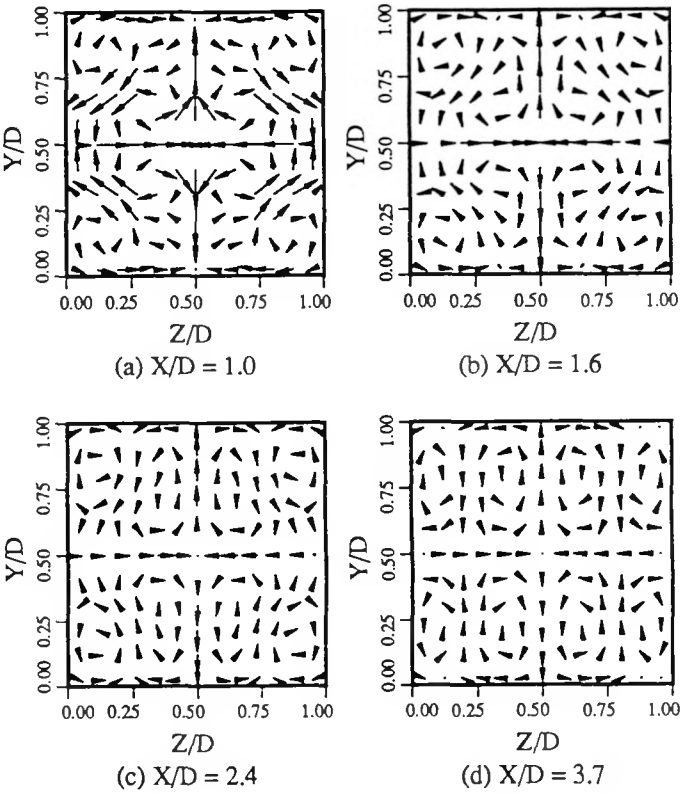

Figure 16 Patterns of secondary flows
(center-8v4h-jet)

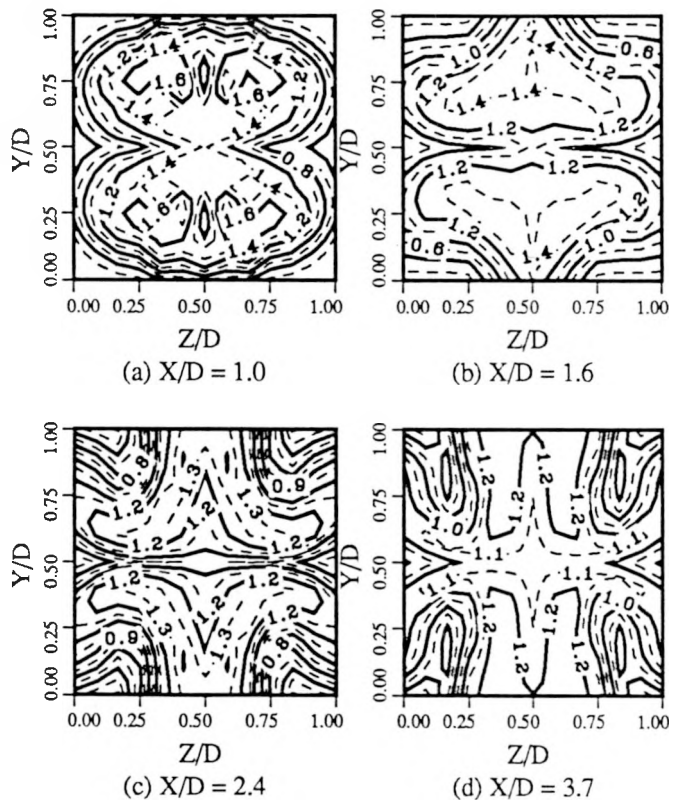

Figure 15 Development of thermal mixing
(β contours, center-8v4h-jet)

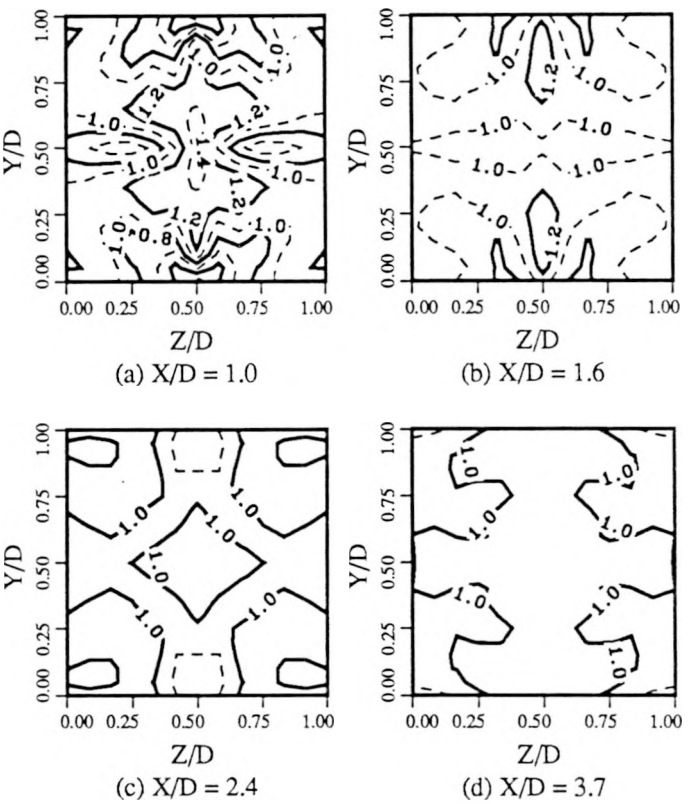

Figure 17 Development of momentum mixing
(U contours, center-8v4h-jet)

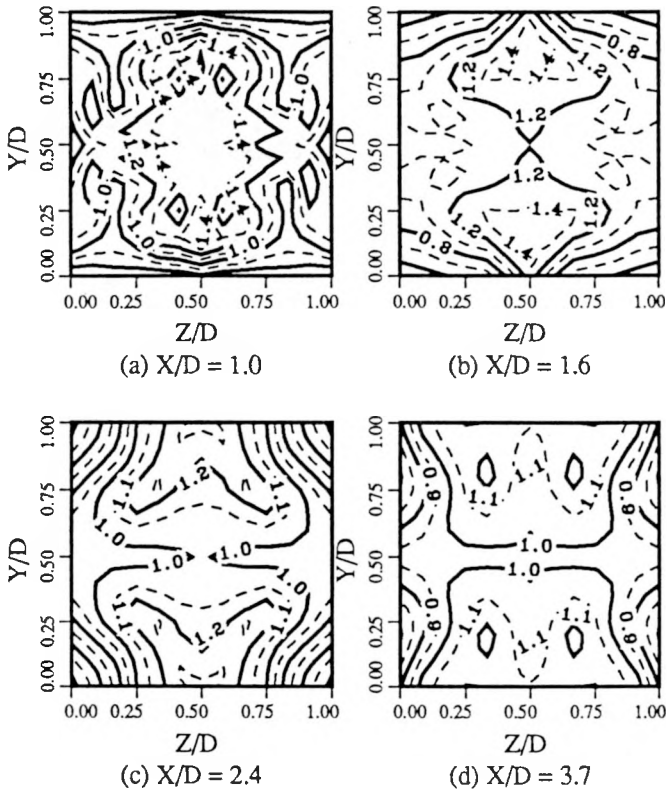

Figure 18 Development of thermal mixing
(β contours, mixed-8v4h-jet)

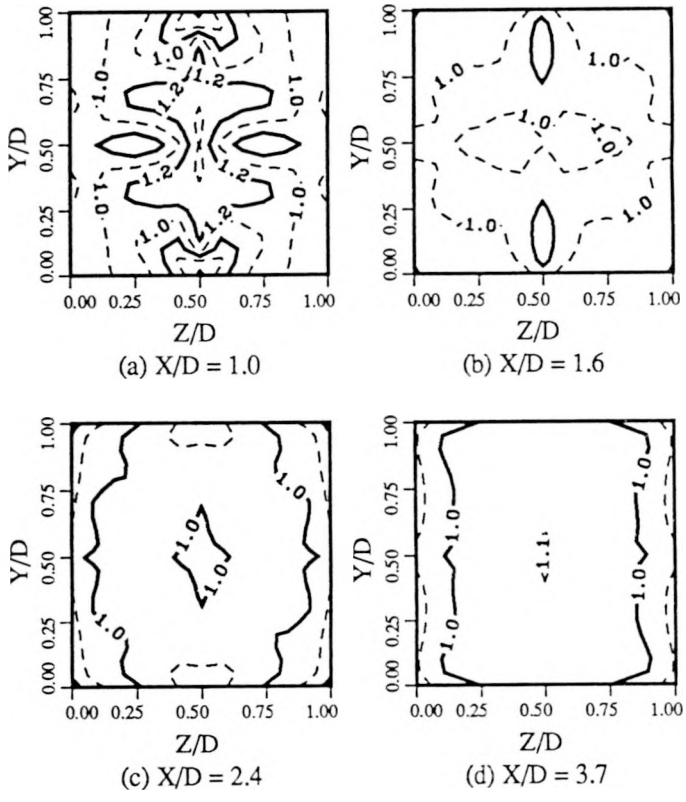

Figure 20 Development of momentum mixing
(U contours, mixed-8v4h-jet)

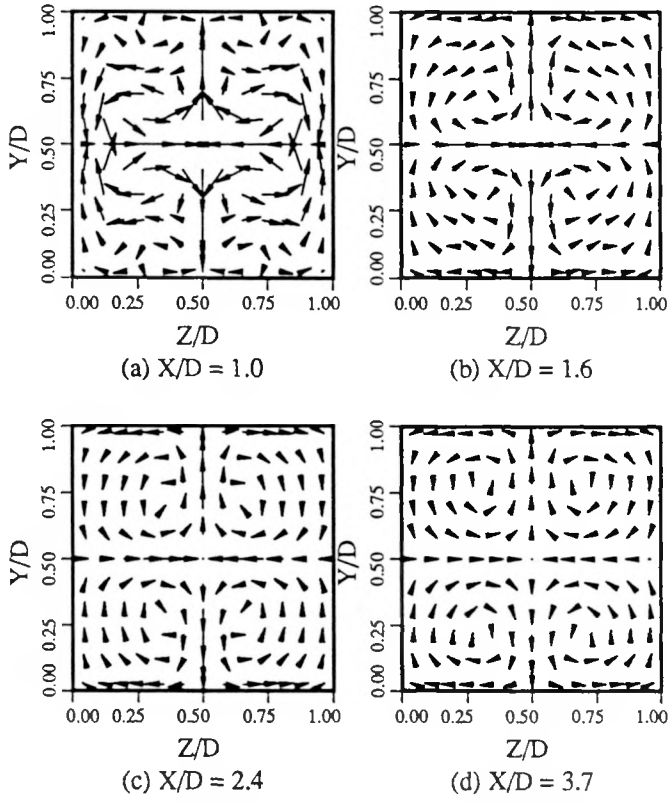

Figure 19 Patterns of secondary flows
(mixed-8v4h-jet)

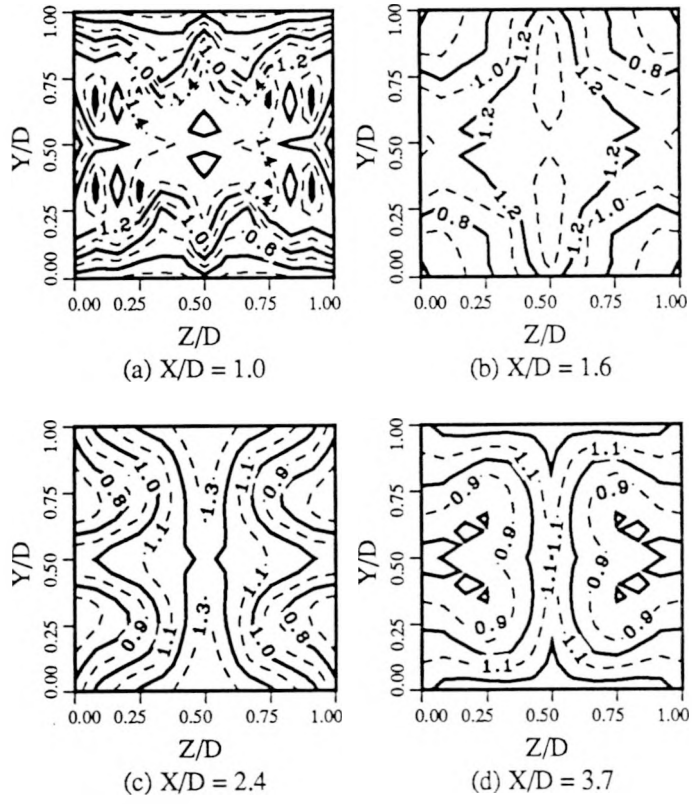

Figure 21 Development of thermal mixing
(β contours, side-8v4h-jet)

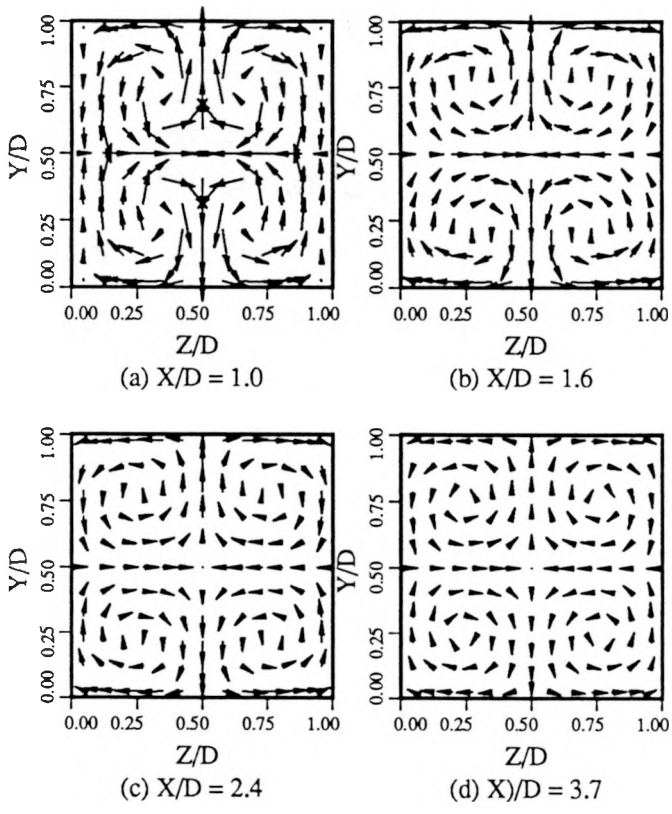

Figure 22 Patterns of secondary flows (side-8v4h-jet)

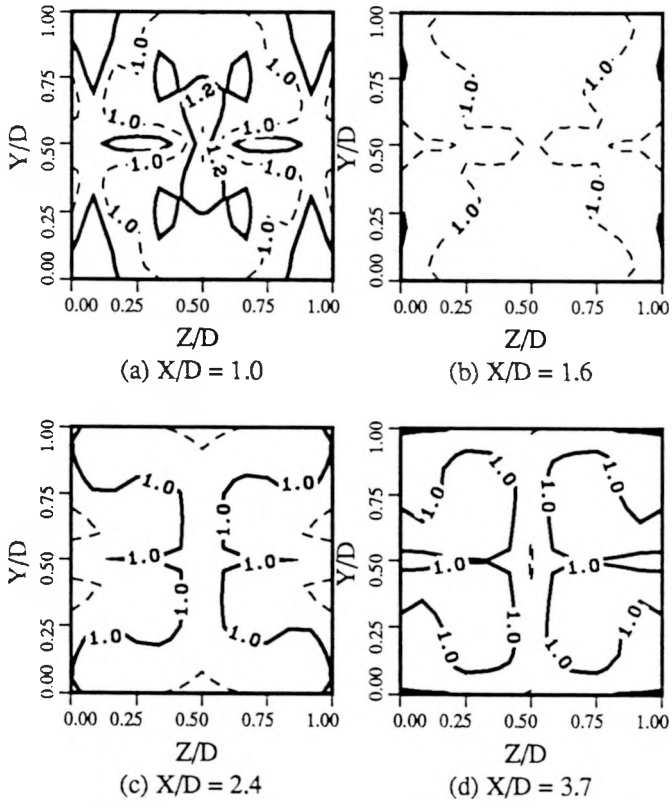

Figure 23 Development of momentum mixing (U contours, side-8v4h-jet)

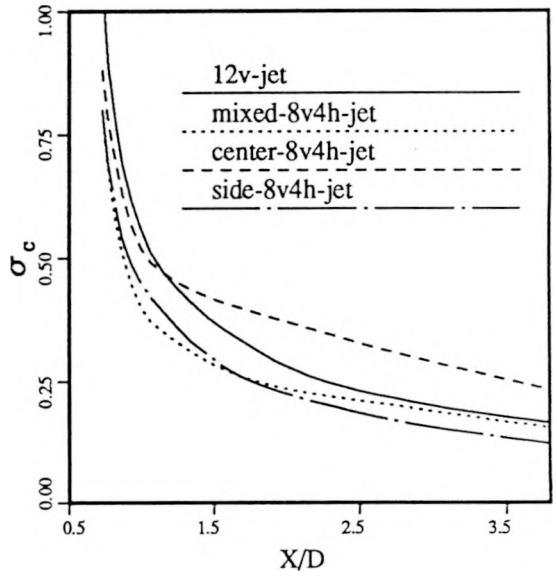

Figure 24 Comparison of fluid mixing development (I)

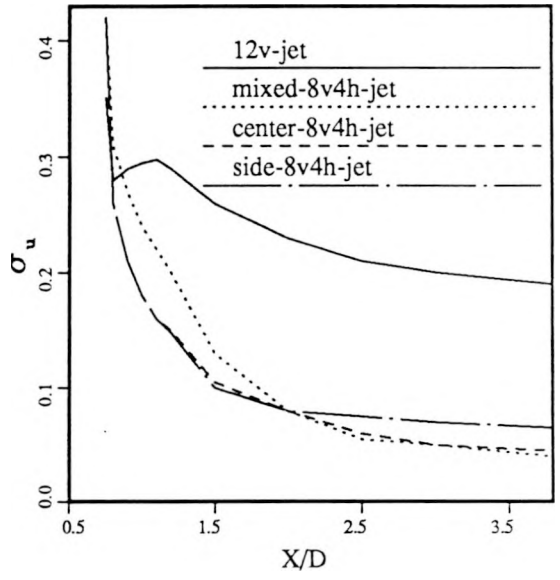

Figure 25 Comparison of momentum mixing development (II)